



Article

RETRACTED: The Influence of Texture on Co/SBA-15 Catalyst Performance for Fischer-Tropsch Synthesis

Jun Han ^{1,2} , Zijiang Xiong ¹, Zelin Zhang ¹, Hongjie Zhang ^{1,*}, Peng Zhou ³ and Fei Yu ^{3,*} 

¹ Hubei Key Laboratory for Efficient Utilization and Agglomeration of Metallurgic Mineral Resources, Wuhan University of Science and Technology, Wuhan 430081, China; hanjun@wust.edu.cn (J.H.); xzj0507@outlook.com (Z.X.); zhangzelin@wust.edu.cn (Z.Z.)

² Industrial Safety Engineering Technology Research Center of Hubei Province, Wuhan University of Science and Technology, Wuhan 430081, China

³ Department of Agricultural and Biological Engineering, Mississippi State University, Mississippi State, MS 39762, USA; zhoupengwust@hotmail.com

* Correspondence: zhanghongjie@wust.edu.cn (H.Z.); fyu@abe.msstate.edu (F.Y.); Tel.: +86-27-6886-2880 (H.Z.)

Received: 28 November 2018; Accepted: 14 December 2018; Published: 16 December 2018



Abstract: The influence of the Co/SBA-15 catalyst texture, such as pore size and pore length on Fischer-Tropsch (FT) Synthesis, was investigated in this paper. The morphology, structure, and microstructures of Co/SBA-15 catalysts were characterized by SEM, Brunauer-Emmett-Teller (BET), TPR, HRTEM, and XRD. The experimental results indicated that the increase of pore size could improve the activity of the Co/SBA-15 catalyst, and the further increase of pore size could not significantly promote the activity. Moreover, it was also found that the pore length of the Co/SBA-15 catalyst played a key role in the catalytic activity. CO₂ and C₄+ selectivity were 2.0% and 74% during the simulated syngas (64% H₂: 32% CO: balanced N₂) FT over the Co/SBA-15 catalysts, and CO conversion rate and CH₄ selectivity were 10.8% and 15.7% after 100 h time on stream.

Keywords: Fischer-Tropsch synthesis; Co/SBA-15; pore size; pore length

1. Introduction

The world's increasing energy demand and the depletion of crude oil has stimulated great interest in Fischer-Tropsch synthesis (FTS), which is a key step in transforming various non-petroleum carbon resources, such as natural gas, coal, and biomass into liquid fuels or valuable chemicals [1-4]. It is well known that Ni [5], Fe [6], Co [7], and Ru [8] are the most active metals for the hydrogenation of carbon monoxide. However, only cobalt-based catalysts and iron-based catalysts have been successfully applied in the industrial FTS application [9]. Cobalt based catalysts are preferred for FTS in a hydrogen rich syngas due to their characteristics of low activity for water-gas shift reaction, high selectivity for linear hydrocarbons, and better resistance to the deactivation by water (a byproduct of FTS reaction) [10,11]. The catalytic properties of the cobalt catalysts are usually affected by the chemical interactions between the supports and cobalt metal, the texture of the catalysts, and crystal morphology. Weak interactions suppress the dispersion of cobalt metal, while strong interactions promote the difficulty of reducing cobalt species. Therefore, a balance of the interactions between the supports and cobalt is significantly important for FTS cobalt-based catalyst [12]. The dispersion of cobalt metal and the surface area of this active ingredient are significantly dependent on the support, and larger particle sizes result in a lower dispersion of metallic Co metallic [13,14].

SBA-15 is a highly ordered mesoporous molecular sieve, which has the characteristics of a narrow pore size distribution (3-30) nm and large surface area (600-1000 m²/g) [15]. Moreover, SBA-15

has uniform hexagonal channels and high thermal stability. The above features of SBA-15 lead to it being regarded as a suitable support for FTS catalyst [16]. Cai et al. and Wang et al. reported that the CO conversion was 6.51%–20.51%, and C⁵⁺ selectivity was 42.43%–77.14% when Ru promoted Co/SBA-15 catalysts was used in FTS [17,18]. García et al. explored the effects of the Co-SiO₂ interaction, and thought that SBA could suppress the aggregation of metal particles and promote the metal dispersion [19].

In this paper, the effect of the texture of Co/SBA-15 on FTS performance was investigated. Moreover, the reaction temperature and Co loading were also discussed.

2. Results and Discussion

SEM images of SBA-15 are presented in Figure 1. SBA-15 consisted of aligned rod-like particles with a diameter of 1 μm and a length of 2–3 μm longwise, which coincided with the results of Prieto et al. [20]. It could be clearly observed from Figure 2 that SBA-15 had a well-ordered hexagonal crystal structure composed of one-dimensional channels, which was highly ordered and stable [21].

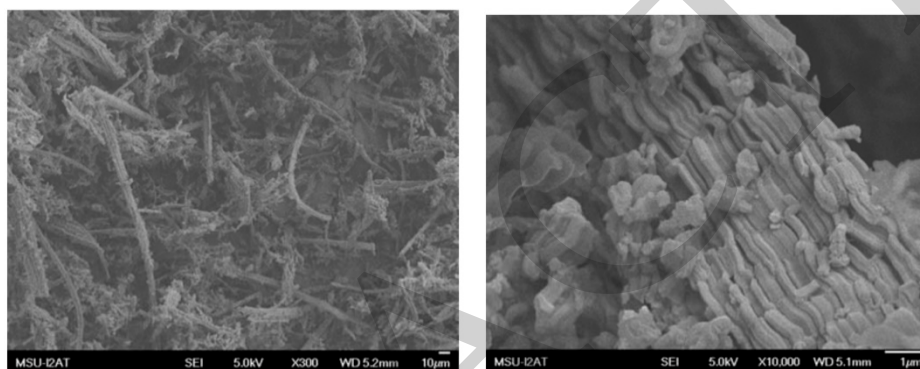


Figure 1. SEM image of SBA-15.

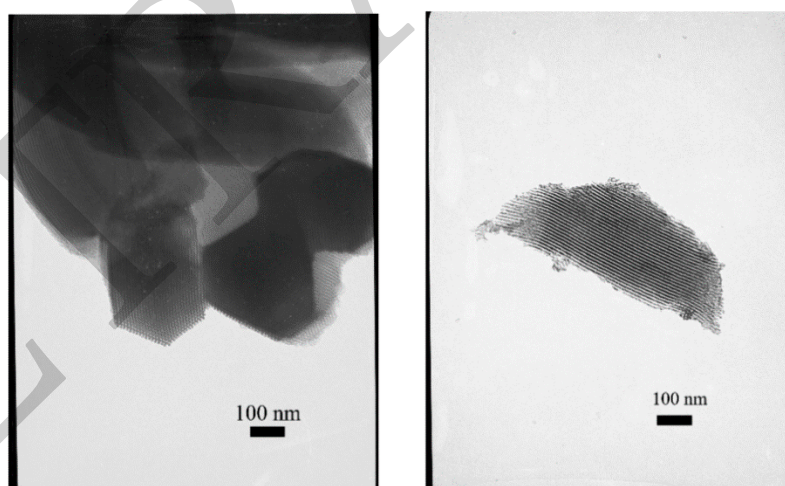


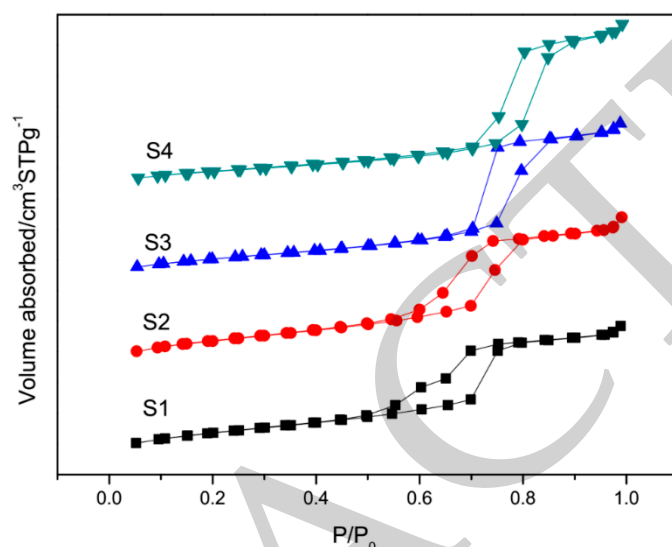
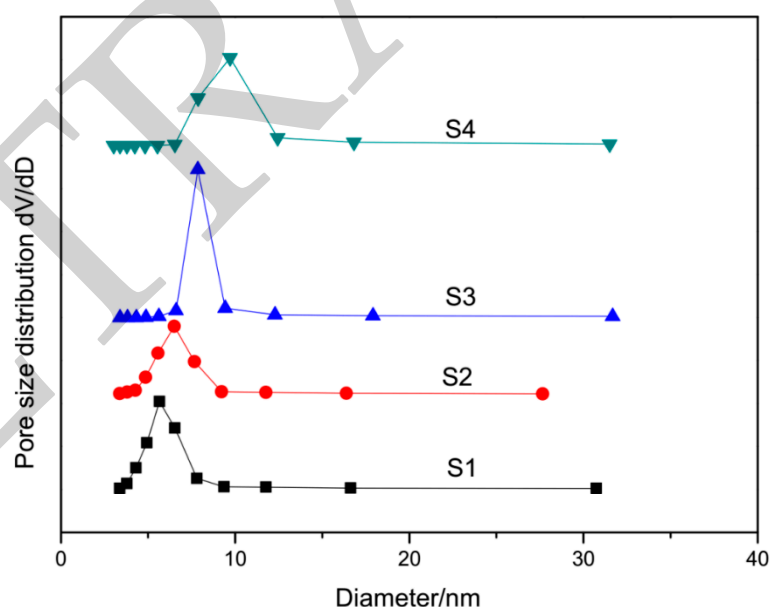
Figure 2. TEM image of SBA-15.

The N₂ adsorption-desorption isotherms and the pore size distributions of Co/SBA-15 catalysts are shown in Figure 3. A type IV adsorption isotherm with a H1 hysteresis loop is observed. The pore size distribution of SBA-15 catalysts Figure 4 demonstrated that Co/SBA-15 catalysts had a narrow pore size distribution. The catalysts that were obtained at 120 °C aging temperature had narrower pore size distributions than the catalysts that were obtained at 100 °C. As shown in Table 1, the average diameters of the SBA-15 catalyst varied from 5 to 10 nm. The pore volume was increased with an increasing average pore diameter, while the surface area of catalyst was decreased with increasing the average pore diameter.

Table 1. Texture properties of 20% Co/SBA-15 catalysts.

Sample	Surface Area (m ² /g)	Pore Diameter (nm)	Pore Volume (cm ³ /g)	Average Pore Length ¹ (μm)
S1	457.5	4.9	0.719	1.6
S2	455.6	6.5	0.802	1.90
S3	395.9	7.9	0.853	1.80
S4	353.7	9.7	0.900	1.70

¹ Estimated by TEM measurements along the pore direction and correction for curved pores.

**Figure 3.** N₂ adsorption-desorption isotherms of Co supported on SBA-15 with different pore sizes.**Figure 4.** Pore size distribution of the catalysts.

The TPR profiles of 20% Co/SBA-15 catalysts with different pore sized are shown Figure 5. The main peak at about 360~390 °C can be attributed to the reduction of Co₃O₄ to CoO, and subsequently to metallic Co. Besides the main peak, two broad reduction peaks at 480~600 °C and 600~850 °C are also observed, which meant that there was the interaction between the surface Co species with the support [22]. As the pore size decreases, the broad peak shifted to the higher

temperature. At the same time, the variation of the main peak was limited. The above results indicated that the catalyst with a smaller pore size was more difficultly reduced. The average crystallite Co_3O_4 particle size was calculated from the Scherrer Equation based on the most intense reflection peak at 36.9°C , as Equation (1). The crystallite size of Co after the reduction could be calculated from the crystallite size of Co_3O_4 , according to Equation (2).

$$D_{\text{Co}_3\text{O}_4} = 0.89\lambda / (\beta \cos \theta) \quad (1)$$

$$D_{\text{Co}} = 0.75D_{\text{Co}_3\text{O}_4} \quad (2)$$

Table 2 presented that the average crystallite size of cobalt particles was increased as the pore size of SBA-15 increases. Xiong et al. thought that the smaller CoO clusters could interact more strongly with the support than the larger ones [22]. Hence, the smaller Co_3O_4 crystallites were reduced with more difficulty than the larger ones [23].

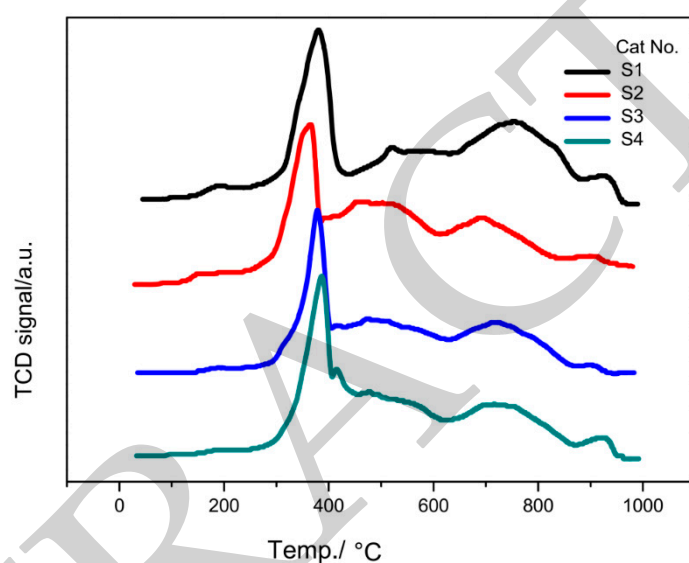


Figure 5. H_2 -TPR profiles of Co/SBA-15 samples with different pore sizes.

Table 2. Average crystalline size of Co_3O_4 estimated by the XRD method.

Sample	Pore Size (nm)	$D_{\text{Co}_3\text{O}_4}$ (nm)	D_{Co} (nm)
S1	4.9	10.5	7.9
S2	6.5	13.8	10.4
S3	7.9	15	11.3
S4	9.7	16	12.0

The XRD patterns in Figure 6 showed there was the diffraction peaks at $2\theta = 0.7^\circ$, which was characteristic of the hexagonal mesoporous structure (p6m) [24,25]. This reflected the ordered structure of SBA-15 was kept after the impregnation of cobalt. The high-angle XRD patterns of catalysts were displayed in Figure 7. Diffraction peaks 31.3, 36.9, 45.1, 59.4, and 65.48 corresponds to the planes (220), (311), (400), (511), and (440) of Co_3O_4 spinel phase (JCPDS 42-1467) [26].

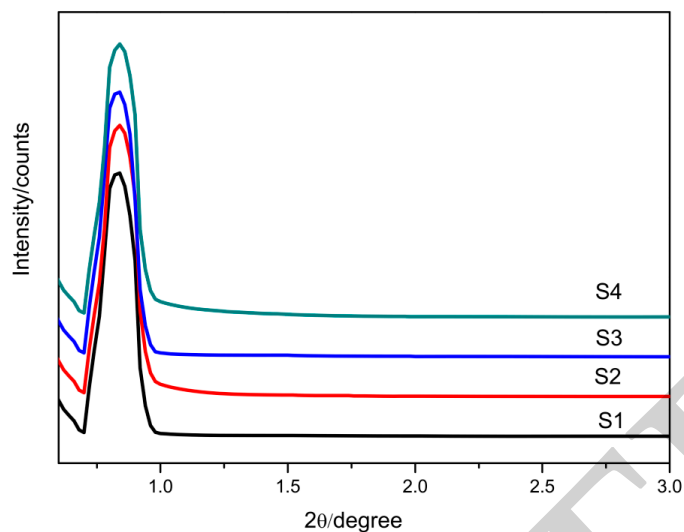


Figure 6. Small-angle XRD pattern of Co/SBA-15 catalyst with different pore sizes.

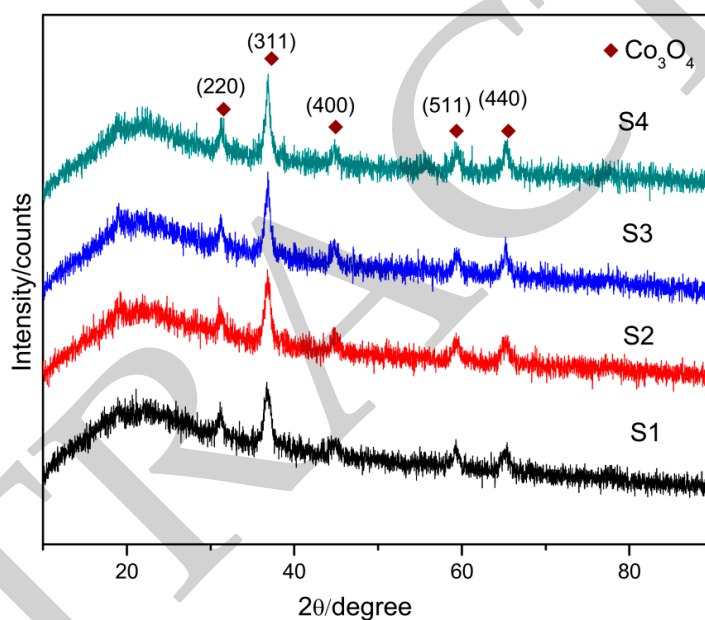


Figure 7. High-angle XRD patterns of the catalysts.

After the comparison of Figures 2 and 8, it was found that the structure of SBA-15 was kept after the cobalt impregnation and calcination. TEM images showed that there were many crystals in the pores, which caused the estimated $D_{\text{Co}_3\text{O}_4}$ in Table 2 to be 10.5–16 nm and to be larger than the pore size of SBA-15. Moreover, Co dispersion in S2 catalyst was more uniform than other catalysts in Figure 8. HRTEM image further confirmed that cobalt was presented in the form of Co_3O_4 crystalline phase after the calcination; (220) planes with a lattice space of 0.287 nm and (400) planes with a lattice space of 0.208 nm were observed for Co_3O_4 .

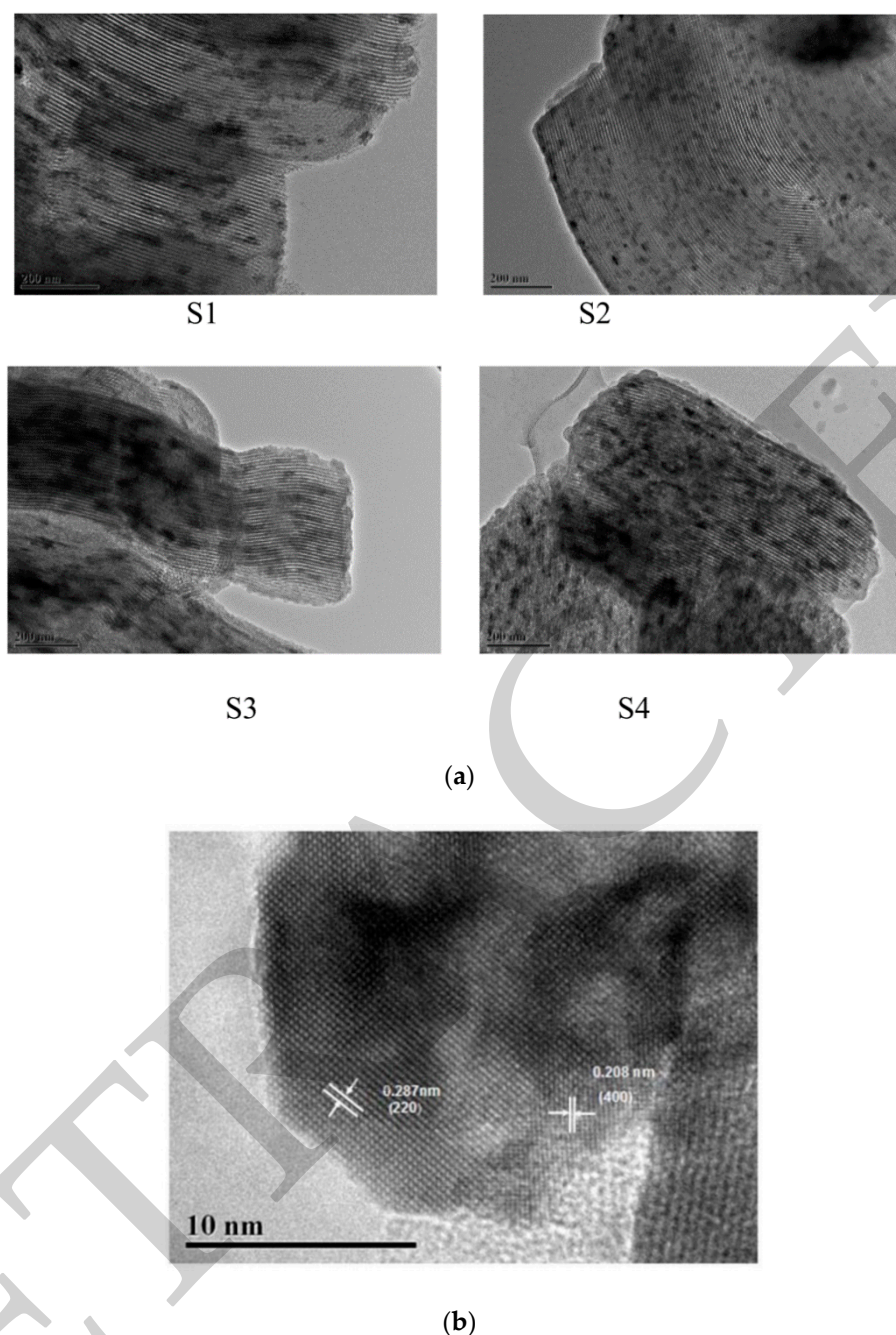


Figure 8. (a) TEM images of calcined 20% Co/SBA-15 catalysts and (b) HRTEM image of Co_3O_4 .

The catalytic performance of Co/SBA-15 catalysts during FTS was evaluated at 215–265 °C and 2 MPa for 15 h. The gas hourly space velocity (GHSV) in all tests was 3600 h⁻¹. Figure 9 presented the influence of the reaction temperature on CO conversion and product selectivity for Co/SBA-15 catalysts with different pore sizes. All Co/SBA-15 catalysts exhibited low CO₂ selectivity and high C₄₊ hydrocarbon selectivity (~80%), which can be attributed to the well pore arrangement of SBA-15. The variation of the pore size in 4.9–10 nm had no obvious effect on C₄₊ selectivity, except for S1 catalyst. The above result was agreed with the previous literatures [13,27]. The larger cobalt particles were formed on the larger pore size of the support, which was easier to form a long chain of hydrocarbon [13]. However, the further increasing the pore size of catalyst had no significant effect on C₄₊ selectivity. Prieto et al. stated the length of the pore in catalyst was more important than the pore size for the catalyst activity [20]. In this test, S2 has the higher CO conversion and C₄₊ selectivity.

The length of S2 catalyst is the longest among the four catalysts. Moreover, the Co particle was more uniformly distributed on SBA-15, as shown in Figure 8.

Figure 9 also presented the increase of reaction temperature that led to a decrease in C4+ selectivity and an increase in methane selectivity. According to the literatures, the destroyed of mesoporous structure of silica and the formation of CoSiO_3 spinel accounted for the decrease of catalytic activity and selectivity. The better performance of the catalysts for C4+ selectivity was thought to be 215 °C.

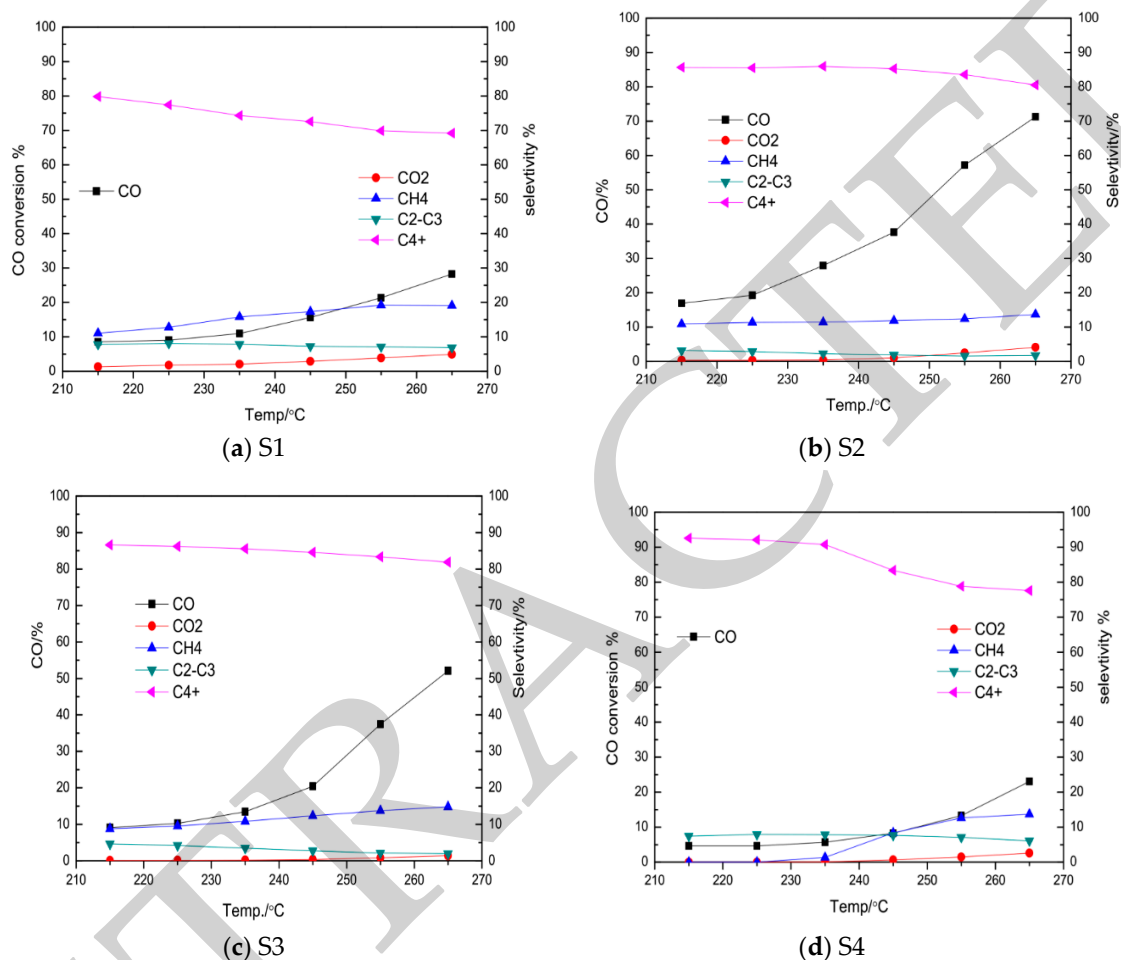


Figure 9. Effect of temperature on CO conversion and product selectivity for the catalysts (a) S1, (b) S2, (c) S3, and (d) S4 with different pore size and length.

S2 catalyst was tested over 100 h to investigate the lifetime activity of the catalyst. Figure 10 illustrated the effects of TOS on the syngas conversion rate and product selectivity at 215 °C. Initially, 12 h after introducing the feed to the reactor, the total conversion of CO and H_2 was about 20%. After 20 h on stream, a constant value was achieved. The overall conversion after 20 h was ~10 mol%. Selectivity towards C4+ was 72% after 20 h and it showed a little increase to 75% after 60 h. Selectivity towards CO_2 and C2–C3 were very low and kept slowly decrease during 100 h. It has reported various mechanisms for the deactivation in cobalt-based FTS, such as the sintering, oxidation of the active Co species, destruction of porous structure, the coke formation, the aggregation of Co particles, poisoning, and cobalt reconstruction [28,29]. Overall, the S2 catalyst displayed good stability and product selectivity over 100 h, which was expected be kept active, even for longer time period.

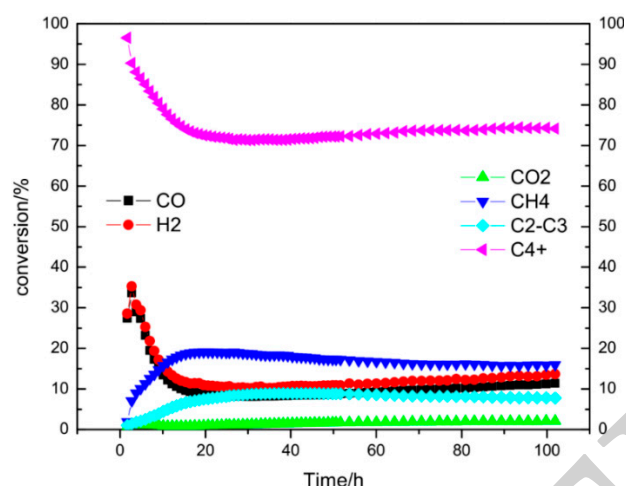


Figure 10. CO conversion rate and CO₂/C₄+ selectivity with time on stream for S2 catalyst.

3. Experimental

3.1. Catalyst Preparation

First, the triblock copolymer (EO₂₀PO₇₀EO₂₀, P123, Sigma Aldrich, 99%, Dorset, UK) was dissolved in the deionized water at room temperature and the solution was stirred for 2 h. Subsequently, HCl (Jiangcheng Chemical Co., Ltd., Wuhan, China) solution was added and stirred for 30 min. and then the required amount of tetraethyl orthosilicate (TEOS, Sigma Aldrich, 98%, Dorset, UK) was added to the above preparation solution at 36 °C and was kept under the stirring for 20 h. Afterwards, the gel mixture was moved into polypropylene bottles and heated at the predetermined aging temperature for the predetermined aging time (As in Table 3). After the synthesis, the solid obtained was filtered, exhaustively washed with the distilled water until neutral pH, dried at 80 °C, and lastly calcined in a flow of air at 500 °C for 6 h to remove the organic template. Co/SBA-15 catalysts were obtained by the incipient wetness impregnation using Co(NO₃)₂·6H₂O/ethanol solution (Sinopharm Chemical Reagent Co., Ltd., Shanghai, China). All of the samples were calcined in air at 450 °C for 6 h (heating rate 1 °C/min) and reduced with H₂ at 400 °C (heating rate 1 °C/min) for 4 h before reaction.

Table 3. The parameters of catalyst preparation.

Sample	Aging Time/h	Aging Temp./°C
S1	24	100
S2	48	100
S3	24	120
S4	48	120

3.2. Catalyst Characterization

The N₂ adsorption–desorption measurements were used to analyze the texture parameters of catalysts by a Micromeritics ASAP 2020 apparatus (Norcross, GA, USA) at −196 °C. The specific surface area was calculated by the Brunauer–Emmett–Teller (BET) method, which N₂-adsorption data was obtained in the relative pressure (P/P_0) range of 0.05–0.30. The total pore volume was determined from the amount of nitrogen at P/P_0 of 0.995. The average pore diameter and pore sizes distribution were obtained by the Barrett–Joyner–Halenda (BJH) method (Micromeritics, Norcross, GA, USA). Before the analysis, the catalysts were degassed at 120 °C for 4 h to remove the impurities from the samples. The reduction characteristic of the oxidized cobalt was studied by the temperature-programmed reduction in a ChemBET Pulsar TPR/TPD (Quantachrome Instruments, Boynton Beach, FL, USA) equipment.

X-ray diffraction patterns (Rigaku, Tokyo, Japan) were investigated at room temperature though monochromatized Cu-K α ($\lambda = 0.15418$ nm) radiation. The average diameters of Co₃O₄ in the catalysts were estimated by the Scherrer Equation. The morphology of supports and catalyst was observed using a field emission scanning electron microscope (FE-SEM) equipped with an energy dispersive X-ray analysis (EDX) detector. A JEOL instrument (Tokyo, Japan) operating at 80 keV or 200 keV was used in this paper.

3.3. Fischer–Tropsch Test

The Fischer–Tropsch synthesis tests were performed in a fixed-bed reactor (diameter is 1/2 inch), which was made with stainless-steel, as shown in Figure 11. Before each experiment, 0.5 g of catalyst was uniformly mixed with quartz sand and was loaded in the reactor. The catalyst was reduced by 50% H₂/N₂ at an atmospheric pressure. During the reduction, the temperature of catalyst was increased to 400 °C with a heating rate of 1 °C min⁻¹ and was maintained at 400 °C for 6 h. After the reduction, the heating was stopped and the temperature was naturally decreased to 120 °C under 50% H₂/N₂. Subsequently, the pressure of the reactor was slowly increased up to 2 MPa by feeding the reactant gases (64% H₂: 32% CO: balanced N₂). Lastly, the temperature of the catalyst was heated to 220 °C (or other designed temperature) at a controlled heating rate of 1 °C/min. In each run, the time of the Fischer–Tropsch reaction was about 10–15 h to evaluate the stabilization and activity of the catalyst. During the reaction, the effluent gases were successively passed two traps to collect waxes, water and the residual products. The off-gas after the cold trap was analyzed by an Agilent 8990 chromatograph.

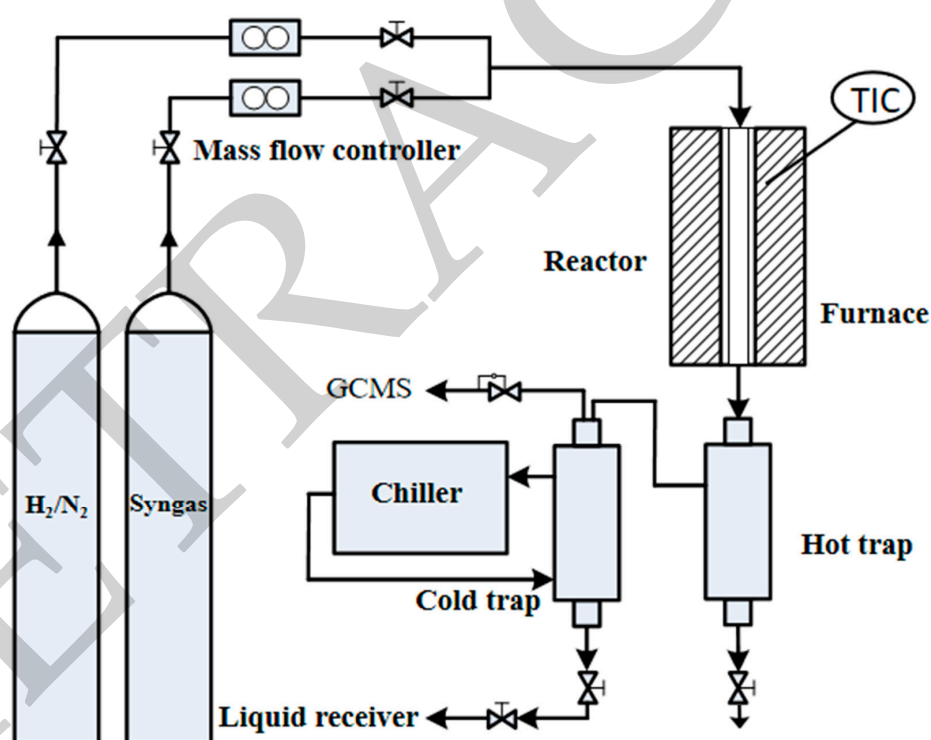


Figure 11. Schematic of experimental setup for FTS.

The CO conversion was defined as Equation (3) and the product selectivity was calculated according to Equations (4). Here, F^0 and F were the flow rates of the feeding syngas and effluent gas, respectively, C_i^0 and C_i were i component concentrations of the feeding syngas and effluent gas, which can be quantitatively analyzed by GC. n was the carbon number in the i species.

$$\text{Conversion of CO (\%)} = \frac{F^0 C_{\text{CO}}^0 - F C_{\text{CO}}}{F^0 C_{\text{CO}}^0} = \frac{C_{\text{CO}}^0 - C_{\text{N}_2}^0 C_{\text{CO}} / C_{\text{N}_2}}{C_{\text{CO}}^0} \times 100 \quad (3)$$

$$\text{Selectivity of product } i \text{ (\%)} = \frac{FC_i n}{F^0 C_{CO}^0 - FC_{CO}} = \frac{C_{N_2}^0 C_i n}{C_{N_2} C_{CO}^0 - C_{N_2}^0 C_{CO}} \times 100 \quad (4)$$

The selectivity of C4+ (S_{C4+}) was determined, as follows:

$$S_{C4+} \text{ (\%)} = 100 - S_{C1} - S_{C2} - S_{C3} \quad (5)$$

4. Conclusions

The influence of texture of the Co/SBA-15 catalyst such as pore size and pore length on Fischer-Tropsch (FT) Synthesis was investigated. The morphology, structure, and microstructures of Co/SBA-15 catalysts were analyzed by SEM, BET, TPR, HRTEM, and XRD. The experimental results demonstrated that the improvement of pore size of the Co/SBA-15 catalyst could improve the activity of catalyst, the further increase of pore size had a limited influence on the activity. However, the pore length was more important to the activity of the Co/SBA-15 catalyst. Moreover, the Co/SBA-15 catalyst had well C4+ selectivity and CO conversion rate during FTS. CO₂ and C4+ selectivity were 2.0% and 74% during the simulated syngas (64% H₂: 32% CO: balanced N₂) FT over the Co/SBA-15 catalysts, and the CO conversion rate and CH₄ selectivity were 10.8% and 15.7% after 100 h time on stream.

Author Contributions: Conceptualization, F.Y. and H.Z.; methodology, J.H.; software, Z.X.; validation, P.Z., J.H. and Z.Z.; formal analysis, P.Z.; investigation, J.H.; writing—original draft preparation, J.H.; writing—review and editing, F.Y.; supervision, F.Y.; project administration, H.Z.; funding acquisition, F.Y., H.Z. and Z.Z.

Funding: This research was funded by Department of Energy under Awards (grant number DE-FG3606GO86025, DE-FC2608NT01923), US Department of Agriculture under Award (grant number AB567370MSU), National Natural Science Foundation of China (grant number 51706160), Foundation of State Key Laboratory of Mineral Processing (grant number BGRIMM-KJSKL-2016-06) and China Postdoctoral Science Foundation (grant number 2017M612522). The APC was funded by National Natural Science Foundation of China (grant number 51706160).

Conflicts of Interest: The authors declare no conflict of interest.

References

- Han, J.; Liang, Y.; Hu, J.; Qin, L.; Street, J.; Lu, Y.; Yu, F. Modeling downdraft biomass gasification process by restricting chemical reaction equilibrium with aspen plus. *Energy Convers. Manag.* **2017**, *153*, 641–648. [[CrossRef](#)]
- Han, J.; Zhang, L.; Lu, Y.; Hu, J.; Cao, B.; Yu, F. The effect of syngas composition on the fischer tropsch synthesis over three-dimensionally ordered macro-porous iron based catalyst. *Mol. Catal.* **2017**, *440*, 175–183. [[CrossRef](#)]
- Han, J.; Zhang, L.; Kim, H.J.; Kasadani, Y.; Li, L.; Shimizu, T. Fast pyrolysis and combustion characteristic of three different brown coals. *Fuel Process. Technol.* **2018**, *176*, 15–20. [[CrossRef](#)]
- Han, J.; Li, W.; Liu, D.; Qin, L.; Chen, W.; Xing, F. Pyrolysis characteristic and mechanism of waste tyre: A thermogravimetry-mass spectrometry analysis. *J. Anal. Appl. Pyrolysis* **2018**, *129*, 1–5. [[CrossRef](#)]
- Saheli, S.; Rezvani, A.R.; Malekzadeh, A. Study of structural and catalytic properties of Ni catalysts prepared from inorganic complex precursor for Fischer-Tropsch synthesis. *J. Mol. Struct.* **2017**, *1144*, 166–172. [[CrossRef](#)]
- Roe, D.P.; Xu, R.; Roberts, C.B. Influence of a carbon nanotube support and supercritical fluid reaction medium on Fe-catalyzed Fischer-Tropsch synthesis. *Appl. Catal. A Gen.* **2017**, *543*, 141–149. [[CrossRef](#)]
- Huang, J.; Qian, W.; Zhang, H.; Ying, W. Influences of ordered mesoporous silica on product distribution over Nb-promoted Cobalt catalyst for Fischer-Tropsch synthesis. *Fuel* **2018**, *216*, 843–851. [[CrossRef](#)]
- Yang, X.; Wang, W.; Wu, L.; Li, X.; Wang, T.; Liao, S. Effect of confinement of TiO₂ nanotubes over the Ru nanoparticles on Fischer-Tropsch synthesis. *Appl. Catal. A Gen.* **2016**, *526*, 45–52. [[CrossRef](#)]
- Luque, R.; Osa, A.R.D.L.; Campelo, J.M.; Romero, A.A.; Valverde, J.L.; Sanchez, P. Design and development of catalysts for biomass-to-liquid-fischer-tropsch (BTL-FT) processes for biofuels production. *Energy Environ. Sci.* **2012**, *5*, 5186–5202. [[CrossRef](#)]

10. Phaahlamohlaka, T.N.; Dlamini, M.W.; Mogodi, M.W.; Kumi, D.O.; Jewell, L.L.; Billing, D.G.; Coville, N.J. A sinter resistant CO Fischer-Tropsch catalyst promoted with Ru and supported on titania encapsulated by mesoporous silica. *Appl. Catal. A Gen.* **2018**, *552*, 129–137. [[CrossRef](#)]
11. Li, Z.; Wu, J.; Yu, J.; Han, D.; Wu, L.; Li, J. Effect of incorporation manner of Zr on the Co/SBA-15 catalyst for the Fischer-Tropsch synthesis. *J. Mol. Catal. A Chem.* **2016**, *424*, 384–392. [[CrossRef](#)]
12. Liu, Y.; Jia, L.; Hou, B.; Sun, D.; Li, D. Cobalt aluminate-modified alumina as a carrier for cobalt in Fischer-Tropsch synthesis. *Appl. Catal. A Gen.* **2017**, *530*, 30–36. [[CrossRef](#)]
13. Intarasiri, S.; Ratana, T.; Sornchamni, T.; Phongaksorn, M.; Tungkamani, S. Effect of pore size diameter of Cobalt supported catalyst on gasoline-diesel selectivity. *Energy Procedia* **2017**, *138*, 1035–1040. [[CrossRef](#)]
14. Rytter, E.; Holmen, A. On the support in Cobalt Fischer-Tropsch synthesis—Emphasis on alumina and aluminates. *Catal. Today* **2016**, *275*, 11–19. [[CrossRef](#)]
15. Liu, J.; Yu, L.; Zhao, Z.; Chen, Y.; Zhu, P.; Wang, C.; Luo, Y.; Xu, C.; Duan, A.; Jiang, G. Potassium-modified molybdenum-containing SBA-15 catalysts for highly efficient production of acetaldehyde and ethylene by the selective oxidation of ethane. *J. Catal.* **2012**, *285*, 134–144. [[CrossRef](#)]
16. Osakoo, N.; Henkel, R.; Loiha, S.; Roessner, F.; Wittayakun, J. Effect of support morphology and Pd promoter on Co/SBA-15 for Fischer-Tropsch synthesis. *Catal. Commun.* **2014**, *56*, 168–173. [[CrossRef](#)]
17. Cai, Q.; Li, J. Catalytic properties of the Ru promoted Co/SBA-15 catalysts for Fischer-Tropsch synthesis. *Catal. Commun.* **2008**, *9*, 2003–2006. [[CrossRef](#)]
18. Wang, Y.; Jiang, Y.; Huang, J.; Liang, J.; Wang, H.; Li, Z.; Wu, J.; Li, M.; Zhao, Y.; Niu, J. Effect of hierarchical crystal structures on the properties of cobalt catalysts for Fischer-Tropsch synthesis. *Fuel* **2016**, *174*, 17–24. [[CrossRef](#)]
19. Wu, L.; Li, Z.; Han, D.; Wu, J.; Zhang, D. A preliminary evaluation of ZSM-5/SBA-15 composite supported Co catalysts for Fischer-Tropsch synthesis. *Fuel Process. Technol.* **2015**, *134*, 449–455. [[CrossRef](#)]
20. Prieto, G.; Martínez, A.; Murciano, R.; Arribas, M.A. Cobalt supported on morphologically tailored SBA-15 mesostructures: The impact of pore length on metal dispersion and catalytic activity in the Fischer-Tropsch synthesis. *Appl. Catal. A Gen.* **2009**, *367*, 146–156. [[CrossRef](#)]
21. Sevimli, F.; Yilmaz, A. Surface functionalization of SBA-15 particles for amoxicillin delivery. *Microporous Mesoporous Mater.* **2012**, *158*, 281–291. [[CrossRef](#)]
22. Xiong, H.; Zhang, Y.; Liew, K.; Li, J. Ruthenium promotion of Co/SBA-15 catalysts with high cobalt loading for Fischer-Tropsch synthesis. *Fuel Process. Technol.* **2009**, *90*, 237–246. [[CrossRef](#)]
23. Carrero, A.; Vizcaino, A.J.; Calles, J.A.; García-Moreno, L. Hydrogen production through glycerol steam reforming using Co catalysts supported on SBA-15 doped with Zr, Ce and La. *J. Energy Chem.* **2017**, *26*, 42–48. [[CrossRef](#)]
24. Zhu, J.; Yang, J.; Miao, R.; Yao, Z.; Zhuang, X.; Feng, X. Nitrogen-enriched, ordered mesoporous carbons for potential electrochemical energy storage. *J. Mater. Chem. A* **2016**, *4*, 2286–2292. [[CrossRef](#)]
25. Han, J.; Zhang, L.; Zhao, B.; Qin, L.; Wang, Y.; Xing, F. The N-doped activated carbon derived from sugarcane bagasse for CO₂ adsorption. *Ind. Crop. Prod.* **2019**, *128*, 290–297. [[CrossRef](#)]
26. Vizcaino, A.J.; Carrero, A.; Calles, J.A. Comparison of ethanol steam reforming using Co and Ni catalysts supported on SBA-15 modified by Ca and Mg. *Fuel Process. Technol.* **2016**, *146*, 99–109. [[CrossRef](#)]
27. Xiong, K.; Zhang, Y.; Li, J.; Liew, K. Catalytic properties of Ru nanoparticles embedded on ordered mesoporous carbon with different pore size in Fischer-Tropsch synthesis. *J. Energy Chem.* **2013**, *22*, 560–566. [[CrossRef](#)]
28. Zhuo, L.; Wu, L.; Han, D.; Wu, J. Characterizations and product distribution of Co-based Fischer-Tropsch catalysts: A comparison of the incorporation manner. *Fuel* **2018**, *220*, 257–263.
29. Kang, J.; Wang, X.; Peng, X.; Yang, Y.; Cheng, K.; Zhang, Q. Mesoporous zeolite Y-supported Co nanoparticles as efficient Fischer-Tropsch catalysts for selective synthesis of diesel fuel. *Ind. Eng. Chem. Res.* **2016**, *55*, 13008–13019. [[CrossRef](#)]

